PERGAMON

Chaos, Solitons and Fractals 13 (2002) 1735–1742

CHAOS
SOLITONS & FRACTALS

www.elsevier.com/locate/chaos

An experimental model to correlate simultaneous body surface and epicardial electropotential recordings *in vivo*

M.P. Nash [a,*,1], C.P. Bradley [a,1], A. Kardos [b], A.J. Pullan [c], D.J. Paterson [a]

[a] *University Laboratory of Physiology, Parks Road, Oxford OX1 3PT, UK*
[b] *Department of Cardiovascular Medicine, John Radcliffe Hospital, Oxford OX3 9DU,UK*
[c] *Department of Engineering Science, The University of Auckland, Auckland, New Zealand*

Abstract

Our aim was to simultaneously record dense arrays of electropotential signals from the heart and body surface of a closed-chest anaesthetised pig during an acute period of regional ventricular ischaemia. After fitting a suture snare to the equatorial region of the left anterior descending (LAD) coronary artery, an electrode sock containing 127 stainless steel contact electrodes (spaced approximately 7 mm apart) was positioned over the ventricular epicardium. The chest was re-closed and fitted an elasticated vest containing 256 ECG electrodes (spaced approximately 15 mm apart). Electrode locations were measured using a mechanical digitising arm and projected onto a customised 3D mathematical model of the porcine torso and heart. Finite element fitted body surface potential maps (BSPMs) and epicardial activation sequences were used to interpret the electropotential signals. Data were sampled at 2 kHz and recorded at 20 s intervals during a four minute period of LAD occlusion, followed by a period of reperfusion and recovery. During occlusion, propagation of epicardial activation slowed monotonically across the ischaemic region and this was clearly associated with a zone of ST segment elevation in the BSPM and Lead V_1 ECG, whilst the Lead II ECG remained relatively unchanged. The epicardial activation sequence had largely recovered after 60 s of reperfusion, although there was still evidence of slowed activation across the ischaemic region compared to the control. Electrocardiac activity had fully restored to its control state after six minutes of reperfusion. Simultaneous recordings of this type will provide an experimental model to be used together with our integrated computational framework to assess the accuracy and sensitivity of activation inverse ECG algorithms during normal and patho-physiological states.

1. Introduction

Non-invasive clinical electrocardiographic imaging has seen little development over the last century. However, several theoretical and computational approaches that attempt to solve the electrocardiographic inverse problem have arisen in the last few decades. Of particular interest is the recent algorithm of Huiskamp and Greensite [1] that attempts to reconstruct the cardiac activation sequence from the time-varying electropotential field recorded at the body surface. What has not been established is the accuracy and sensitivity of this algorithm under normal conditions and during various patho-physiological states that are encountered in the clinical setting. The primary objective of our research programme is to further develop and quantitatively validate the activation inverse approach (as well as other inverse approaches, based on epicardial potentials) using a combination of in vivo experimental recordings and computational analysis.

* Corresponding author. Tel.: +44-1865-272547; fax: +44-1865-282170.
E-mail address: martyn.nash@physiol.ox.ac.uk (M.P. Nash).
[1] Both authors contributed equally to this study.

0960-0779/02/$ - see front matter
PII: S0960-0779(01)00165-5

The specific aim of this study was to investigate the effects of regional ischaemia on the electrocardiac activity recorded simultaneously from the heart and body surface of a closed-chest anaesthetised pig. We have previously described effects of epicardial pacing on ventricular activation and the associated body surface potential maps (BSPMs) [2]. Taken together, these studies form part of our database of controlled physiological interventions that can be used to validate and refine the computational inverse ECG approach.

2. Methods

Anaesthesia, surgical procedures and electropotential mapping methods have been fully described previously [3], but are briefly summarised here. The investigation conforms to the Guide for the Care and Use of Laboratory Animals published by the US National Institutes of Health [DHEW publication no. (NIH) 85-23, revised 1996, Office of Science and Health Reports, DRR/NIH, Bethesda MD 20205] and was performed in accordance with the British Home Office licence requirements (PPL 30/1133, Queen Anne's Gate, London) and the Animals (Scientific Procedures) Act 1986 (UK).

2.1. Anaesthesia and haemodynamic measurements

A 29 kg domestic pig was anaesthetised with 2–3% halothane (Fluothane, ICI), for induction, and bolus infusions of alpha-chloralose (Sigma, 100 mg/kg i.v., repeated approximately every two hours as required), for maintenance. Femoral arteries and veins were cannulated and arterial blood pressure (ABP) and the Lead II ECG were monitored. Core temperature and arterial blood gases and pH were maintained at physiological values. ABP was measured using a saline-filled pressure transducer (SensoNor 840, Norway) connected to a real-time data acquisition system (MP 100, Biopac Systems) employing Acqknowledge 3.0 software for the Macintosh (Macintosh Quadra 950). Heart rate (HR) was computed using this software.

2.2. Measurement of in vivo heart geometry

Three-dimensional (3D) ultrasound (HPSONOS 5500) was used pre-operatively to obtain the size, orientation and location of the heart within the torso. The image sets were manually digitised and segmented to provide parametric 3D representations of the ventricular surfaces (see Fig. 1). A mechanical digitising arm (FARO Technologies) was used to record the position and orientation of the 3D ultrasound probe in order to quantitatively register the ultrasound image

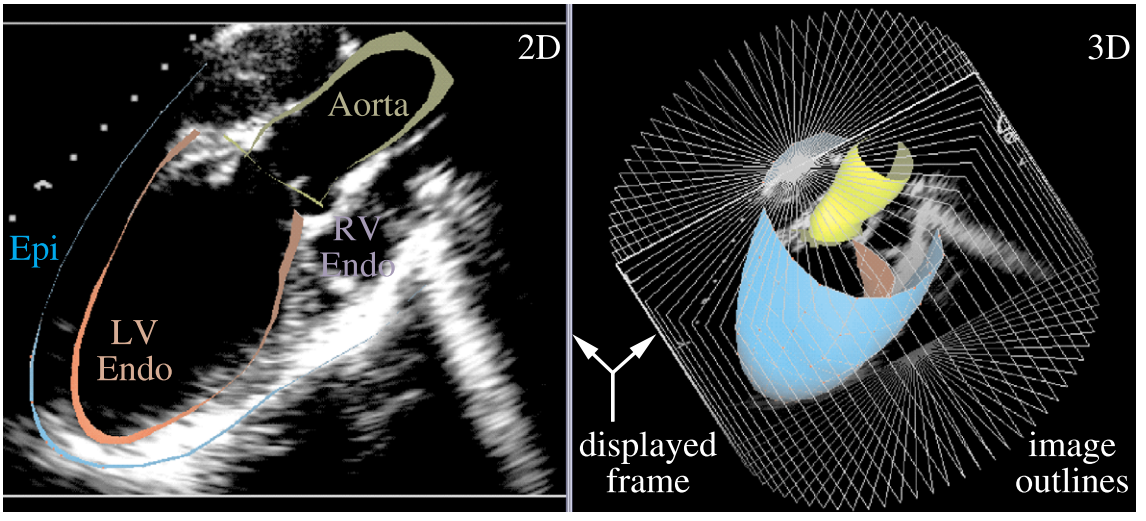

Fig. 1. 3D echocardiographic imaging and ventricular model segmentation. Thirty-seven axially aligned images were captured and registered in 3D (right panel) with respect to a pre-defined anatomical frame of reference. The 3D image set was used to construct parametric descriptions of the epicardial (Epi), LV endocardial (LV Endo) and RV endocardial (RV Endo) surfaces.

sets with respect to a pre-defined anatomical frame of reference. In this way, the experimental heart geometry was located inside a customised computational torso model (described below). These data are of central importance for the ECG inverse validation studies, since computational predictions of the electrical field at the body surface are dependent on the shape, size and orientation of the electrical source (i.e. the heart).

2.3. Surgery and electropotential mapping

The anaesthetised pig was tracheotomised, artificially ventilated (Oxford Mark II ventilator, Penlon), thoracotomised and pericardectomised. The left anterior descending (LAD) coronary artery was ligated (but not occluded at this stage) equatorially using a suture snare (Ethicon, 3-0 mersilk). An elasticised sock containing 127 unipolar stainless steel electrodes (inter-electrode spacing approximately 7 mm; Biomedical Instruments Designers, Montreal) was slipped over the ventricles. The chest was then re-closed (the epicardial electrode wires and suture snare exited near the diaphragm) and filled with saline to eliminate air pockets. A custom-made vest containing 256 electrodes (inter-electrode spacing approximately 15 mm) was then fitted to the animal. Electrodes on the epicardial sock and torso vest were connected to a 448 channel Unemap cardiac mapping system (Uniservices, Auckland, New Zealand). Simultaneous arrays of body surface and epicardial unipolar electropotential signals were recorded at 2 kHz. All signals were referred to the Wilson's central terminal (WCT; electrical average of the signals recorded from both front and the left-rear limbs), whilst the right-rear limb was driven by the negative of the WCT signal (''right leg drive'') to increase the signal-to-noise ratio.

2.4. Protocol

Control measurements were recorded before four minutes of LAD occlusion. From the start of occlusion, ventricular epicardial and body surface electropotentials were simultaneously sampled at 20 s intervals and recordings were continued for three minutes after reperfusion. One final recording was taken 10 minutes after the LAD was first occluded (i.e. following six minutes of reperfusion).

2.5. Localisation of the torso and epicardial electrodes

The FARO arm was used to directly record the majority (approximately 85%) of the 3D locations of the torso electrodes. The remaining torso electrodes, situated on the back of the animal, could not be directly digitised. Therefore, their positions were interpolated from the known organisation of the electrodes on the vest, together with the measured positions of the nearest obtainable neighbours.

After completing the protocol for this study, the chest was carefully re-opened and approximately 45% of the epicardial sock electrodes were digitised using the FARO arm. In a similar manner to the hidden torso electrodes, the unknown epicardial electrode locations were estimated from the known electrode positions together with the pre-defined electrode topography of the epicardial sock.

2.6. Generic computational model of the porcine torso

We constructed an anatomically accurate generic model of the pig by first placing an animal in a CT scanner and recording a sequence of cross-sectional images. These images were manually digitised to provide 3D data sets for the endocardial, epicardial, lungs and skin (torso) surfaces. A non-linear optimisation procedure, which incorporated non-linear constraints and smoothing, was used to obtain a parametric 3D representation for each surface. C^1 cubic Hermite elements were used to define the smoothly continuous anatomical geometry. Further information regarding the evelopment of the generic porcine torso model may be found in [4,5] and for full details of the geometric fitting procedure, refer to [6].

2.7. Torso model customisation

The generic torso model was customised to provide a computational model for the specific animal, as illustrated in Fig. 2. This was achieved by first using the FARO arm to locate a number of anatomical landmarks on the animal and hence set up an anatomical frame of reference. The same anatomical landmarks were identified on the generic torso model and a non-linear host mesh fitting procedure, which minimised the differences between the two sets of anatomical landmarks, was used to transform the generic model into the customised torso model. Further information on the torso customisation procedure may be found in [4,5].

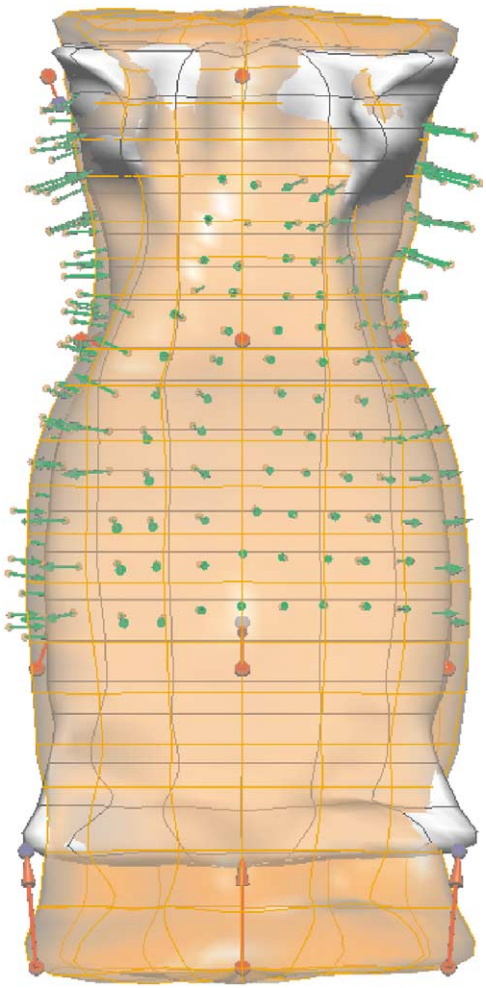

Fig. 2. Anterior (chest) view of the customised computational torso model. The generic torso mesh (inner grey surface) was customised into the experimental model (opaque orange surface) by minimising the differences between anatomical landmarks located on the generic model (blue spots) and on the experimental animal (red spots; red arrows show the landmark translations). Torso electrode locations (orange spots) were projected onto the customised mesh (green arrows show perpendicular projections) as part of the body surface potential mapping process. Top, neck; bottom, abdomen.

2.8. Torso and epicardial mapping

The customised torso model and measured vest electrode locations were used to interpret the recorded body surface ECGs. First, the measured 3D torso electrode locations were perpendicularly projected onto the customised torso model. Secondly, a single cycle of electrocardiac activity was identified using the Unemap software and a 500 Hz low-pass filter was applied to reduce noise. The raw signals were then baselined to define the zero reference immediately prior to the P wave of the Lead II ECG. Finally, a scalar body surface potential field was fitted for each temporal sample and the fitted fields were collated to produce an integrated spatio-temporal description of the electropotential changes at the torso surface. BSPMs were displayed on the customised torso model using a colour spectrum to represent electropotential values (e.g. see Fig. 3).

The echocardiographically derived heart model and the 3D locations of the sock electrodes were used to interpret the in vivo epicardial surface electropotential signals. First, the known topographical organisation of the electrode sock was used to estimate epicardial electrode locations on the surface of the heart model (using a similar technique to the vest electrode projection process). Secondly, a single cycle of electrocardiac activity was identified using the Unemap software (the epicardial signals did not require filtering) and the activation time for each electrode was determined using

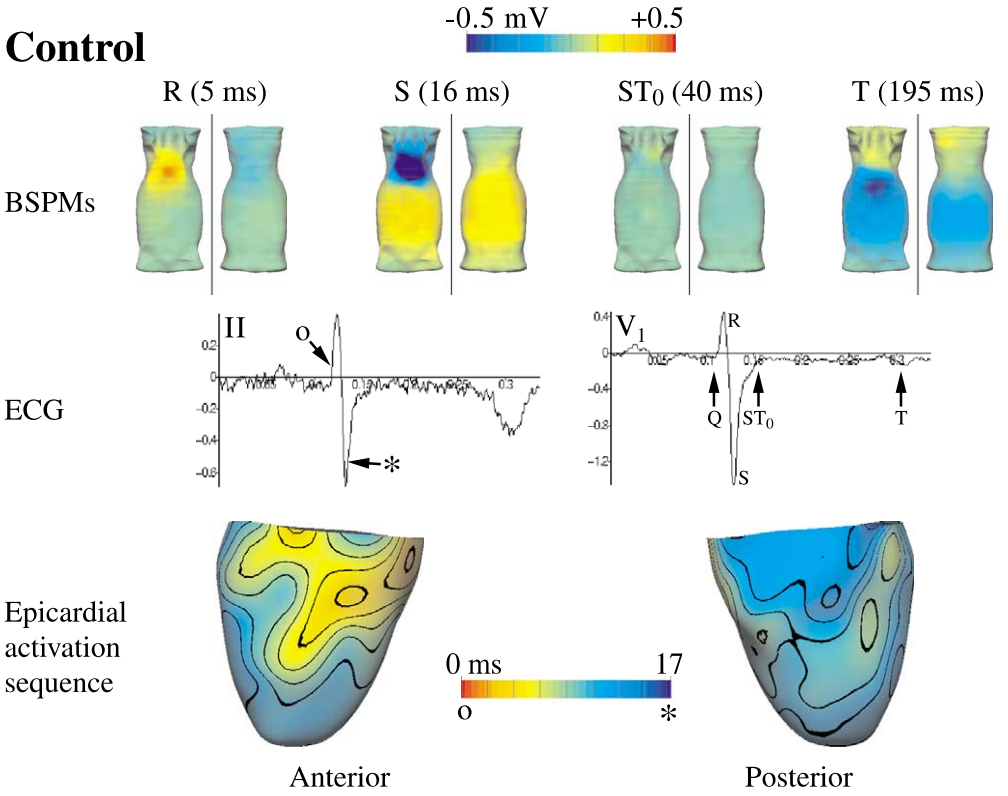

Fig. 3. Simultaneous torso and ventricular electrocardiac activity during normal sinus rhythm. Top panels show anterior (left) and posterior (right) views of the body surface potential maps (BSPMs) for the R, S, ST_0 and T waves of the Lead V_1 ECG (middle-right panel). Times between these events and the beginning of the QRS complex are shown in parentheses. Earliest (red, ○) and latest (blue, ∗) times for the underlying epicardial activation sequence (bottom panels) are shown on the Lead II ECG (middle-left panel). See text for further explanation.

the most negative electropotential slope. Finally, a smoothly varying scalar field was fitted to the epicardial electrode activation times and displayed on the customised heart model using a pseudo-colour spectrum and contour bands to indicate the epicardial activation sequence.

3. Results

3.1. Sinus rhythm

The epicardial activation sequence during normal sinus rhythm is illustrated in Fig. 3. Normal epicardial activation progressed from the mid-anterior regions of the ventricles (where the wall is thinnest), to the thicker postero-basal region in 17 ms. Control BSPMs are illustrated for the R, S, ST_0 (defined as the beginning of the ST segment) and T waves of the Lead V_1 ECG. The BSPM at R contained a region of positivity (red) on the anterior (chest) surface. A large region of anterior negativity (blue) appeared at S and, to a lesser extent, during the T wave.

3.2. Regional ischaemia

After 60 s of LAD occlusion (see Fig. 4), the Lead V_1 ECG showed a significant ST segment elevation and a much more pronounced T wave compared to control. This correlated with anterior regions of positivity in the BSPM at ST_0 and T. The regional ischaemia resulted in a zone of slowed activation on the anterior wall of the ventricles (distal to the

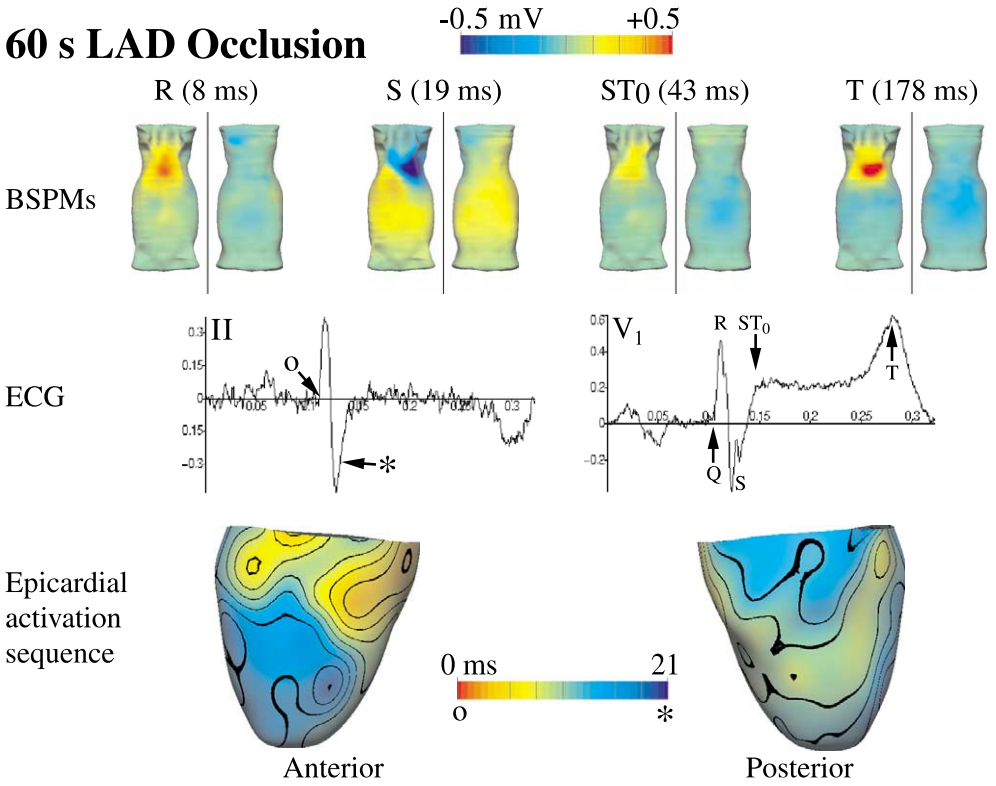

Fig. 4. Simultaneous torso and ventricular electrocardiac activity after 60 s of LAD occlusion. See text and Fig. 3 legend for explanation.

suture snare), leading to an increase in the dispersion of epicardial activation from 17 ms (control) to 21 ms. This alteration to the cardiac activation sequence was associated with a reduction in the area of anterior negativity of the BSPM at S. The morphology of the Lead II ECG was similar to the control recording.

Four minutes of regional ischaemia resulted in dramatic alterations to the epicardial activation sequence, with an anterior region of slowed activation (see Fig. 5; dispersion of ventricular epicardial activation was 36 ms) compared to the control (17 ms). This caused an even greater elevation of the ST segment and gross changes to the morphology of the Lead V_1 ECG for the excitation and repolarisation phases of the cycle, whilst the Lead II ECG was again similar to the control. Large areas of anterior positivity in the BSPM at ST_0 and T were associated with this ventricular electrical disturbance. Subtle changes in the BSPM at S were also observed in comparison to the BSPM after 60 s of LAD occlusion.

3.3. Reperfusion and recovery

Electrocardiac activity had largely recovered 60 s after the LAD snare was released, as illustrated in Fig. 6. The Lead V_1 ECG was similar to the control morphology, as was the BSPM at ST_0 and T. The ventricular activation sequence had not fully recovered by this stage, as shown by the anterior region of slowed activation compared to the control. This was also evident in the BSPM at S, which also had not fully recovered. Ventricular activation and the BSPM at S were fully restored after six minutes of reperfusion (not shown). Ventricular arrhythmia was not observed at any stage during reperfusion.

4. Conclusions and critique

We have illustrated the evolution of the cardiac electrical disturbance due to localised ventricular ischaemia using simultaneous in vivo recordings of epicardial and body surface electropotential activity. Significant differences

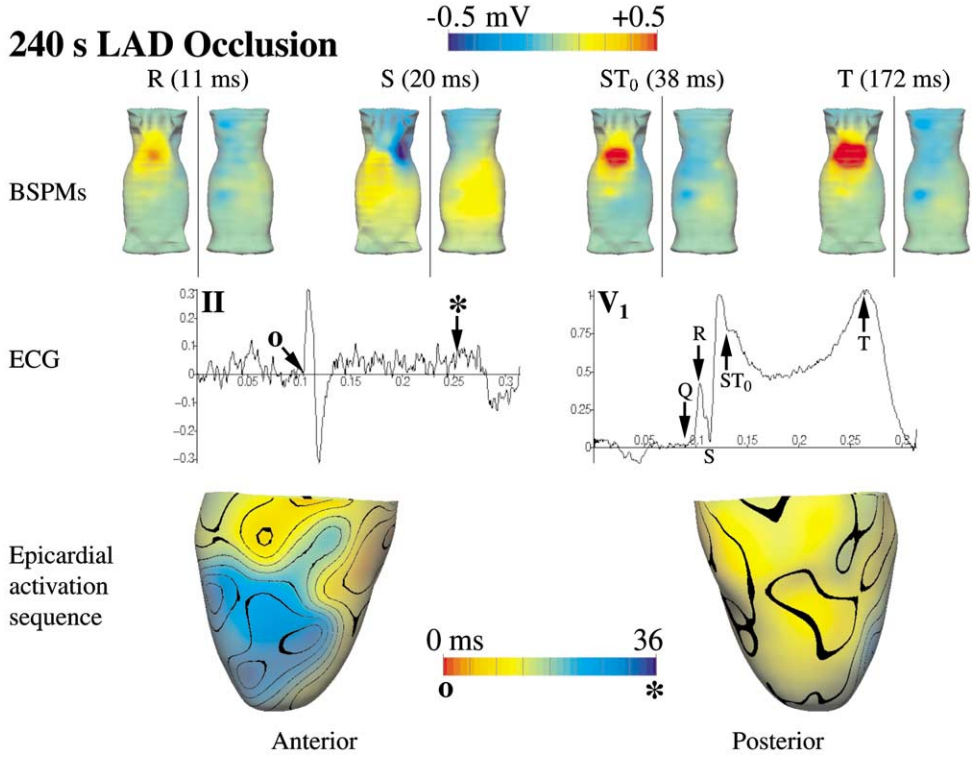

Fig. 5. Simultaneous torso and ventricular electrocardiac activity after 240 s of LAD occlusion. See text and Fig. 3 legend for explanation.

in the ventricular activation sequence, BSPMs and Lead V_1 ECG were observed after one minute of LAD occlusion, and activation across the ischaemic region progressively slowed during the four minute insult. Associated with these changes were a significant ST segment elevation of the Lead V_1 ECG and an anterior region of positivity of the BSPM that was not present under control conditions. In contrast, the morphology of the Lead II ECG remained relatively unchanged during the entire protocol, illustrating how the electrical state of the heart cannot always be determined by monitoring a single ECG lead. Extending this concept, it is then likely that BSPMs with dense arrays of torso ECGs will enable the detection of more subtle electrocardiac changes, in comparison to the standard 12-lead ECG. Furthermore, the use of validated computational inverse approaches to interpret the BSPMs could enable better localisation of the electrocardiac abnormalities than can be deduced from 12 leads.

The protocols and data presented in this manuscript form part of an integrated experimental and computational framework we have developed to investigate the accuracy and suitability of an inverse ECG algorithm that attempts to non-invasively reconstruct the cardiac activation sequence from densely sampled ECG recordings at the body surface. Perhaps the most difficult geometrical data to acquire, and hence the biggest source of error in our experimental paradigm, were the accurate localisation of the epicardial sock electrodes within the closed chest. As the chest was re-opened, there was likely to have been some small movement of the heart, but this remains unquantified. We assumed this movement to be negligible, but the exact locations of individual in vivo epicardial recordings has not been firmly established. During more recent studies, we have integrated a sonomicrometry system (Sonometrics, Canada) into our experimental paradigm in order to more accurately determine the locations of individual epicardial electrodes within the closed chest to reduce the errors in electrode localisation.

In conclusion, we plan to use our database of simultaneous recordings of electrocardiac and body surface activity to assess the accuracy of a computational ECG inverse approach. Using data of the type in this study, we will also investigate the sensitivity of the algorithm with respect to errors in both signal and geometric measurements, in order to determine the suitability of the activation inverse approach to the clinical environment.

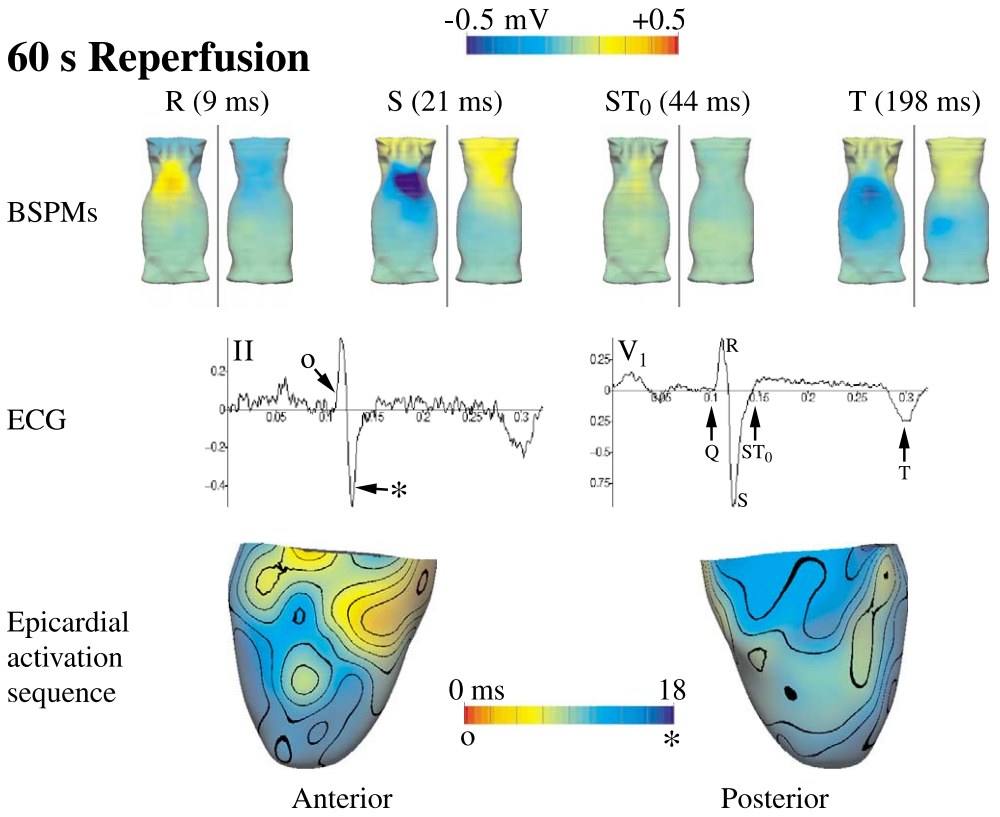

Fig. 6. Simultaneous torso and ventricular electrocardiac activity following 60 s of reperfusion. See text and Fig. 3 legend for explanation.

Acknowledgements

This work was funded by the Wellcome Trust and the British Heart Foundation. Much of the torso model customisation work was first implemented by Leo Cheng, who was also involved in the development of the activation inverse ECG method. We appreciate the advice and expertise of Gerardo Sanchez-Ortiz and Jerome Declerck regarding the echocardiographic studies and analysis, and thank Chris Hirst and Vivienne Harris for their technical support.

References

[1] Huiskamp G, Greensite F. A new method for myocardial activation imaging. IEEE Trans Biomed Eng 1997;44:433–46.
[2] Nash MP, Bradley CP, Cheng LK, Pullan AJ, Paterson DJ. An experimental–computational framework for validating in-vivo ECG inverse methods. Int J Bioelectromagnetism 2000;2 (2) [http://www.tut.fi/ijbem/].
[3] Nash MP, Thornton JM, Sears CE, Varghese A, O'Neill M, Paterson DJ. Ventricular activation during sympathetic imbalance and its computational reconstruction. J Appl Physiol 2001;90(1):287–98.
[4] Cheng LK, Pullan AJ. Towards non-invasive electrical heart imaging. In: Proceedings of the First Joint Meeting of BMES and IEEE/EMBS, Atlanta, GA, 1999. p. 57.
[5] Pullan AJ, Cheng LK, Nash MP, Bradley CP, Paterson DJ. Non-invasive electrical imaging of the heart – theory and model development. Ann Biomed Eng 2001 [in press].
[6] Bradley CP, Pullan AJ, Hunter PJ. Geometric modelling of the human torso using cubic Hermite elements. Ann Biomed Eng 1997;25:96–111.